Supporting Information

Metal Assisted Core-shell Plasmonic Nanoparticle for Small Molecule Biothiols Analysis and Enantioselective Recognition

Meihuang Zeng,[a] Linmin Chen,[a] Xiaocong Hou,[b] Jingwen Jin,[b] Qiuhong Yao,[b] Tingxiu Ye,[d] Zhiyong Guo,*[b, e] Xiaomei Chen,*[a] Xi Chen*[c]

[a]*College of Ocean Food and Biological Engineering, Jimei University, Xiamen 361021, China. E-mail: xmchen@jmu.edu.cn*

[b]*Institute of Analytical Technology and Smart Instruments and Colleague of Environment and Public Healthy, Xiamen Huaxia University, Xiamen, 361024, China. E-mail: guozy@hxxy.edu.cn*

[c]*State Key Laboratory of Marine Environmental Science, Xiamen University, Xiamen 361005, China. E-mail: xichen@xmu.edu.cn*

[d]*College of Pharmacy, Xiamen Medicine College, Xiamen 361005, China*

[e]*Xiamen Environmental Monitoring Engineering Technology Research Center*

* Corresponding authors.

Supplementary material

1.1 Materials

All chemicals including gold (III) chloride trihydrate ($HAuCl_4\,3H_2O$, ≥99.9%), sodium citrate ($C_6H_5O_7Na_3$, 98%), NaCl (Sodium chloride, 99.5%), KOH (Potassium hydroxide, 99.99%), $CaCl_2$ (Calcium chloride anhydrous, 96%), $MgCl_2$ (Magnesium chloride, 99%), L-Tryptophan ($C_{11}H_{12}N_2O_2$, 99%), L-Cysteine ($C_3H_7NO_2S$, 98%), L-Proline($C_5H_9NO_2$, 99%), L-Leucine($C_6H_{13}NO_2$, 99%), L-Tyrosine($C_9H_{11}NO_3$, 99%), D-Leucine($C_6H_{13}NO_2$, 99%), aminoethylpiperazine (AEP), propane cyclic lactone (1,3-PS), D-Proline($C_5H_9NO_2$,99%), DL-homocysteine($C_8H_{16}N_2O_4S_2$, 95%), D-Tyrosine ($C_9H_{11}NO_3$, 98%), D-Cysteine($C_3H_7NO_2S$, 98%), Ethanol anhydrous (99.5%), acetone, acetonitrile, Glutathione($C_{10}H_{17}N_3O_6S$, 99%), D-Tryptophan ($C_{11}H_{12}N_2O_2$, 98%), 3-Hydroxytyraminehydrochloride ($C_8H_{11}NO_2{\cdot}HCl$, 98%) were purchased from Aladdin Chemical Reagent Co. Ltd. (Shanghai, China). All other reagents were at least analytical reagent grade and performed without further purification. Ultrapure water (resistivity up to 18.2 MΩ) was used throughout the experiment.

1.2 Apparatus

Spectrum behaviors study. Optical behaviors and sensing tests based on Cu-APM biosensor were confirmed using an ultraviolet visible spectrometer (UV-2600i, Shimadzu), SERS spectroscopy (ATR8300AF, Aoputiancheng, China), and Fourier transform infrared spectroscopy (FTIR, Nicolet iS50 FTIR spectrometer, USA). SERS measurements were performed with an ATR8300AF autofocus micro-Raman spectrometer with an integration time of 6000 ms, laser power of 50 mW, excitation

wavelength of 785 nm and 20x objective. These tests were repeated for three times with each sample.

Morphology characterizations. The morphology of the Cu-APM biosensor was characterized by transmission electron microscopes (TEM, Tecnai-G2-F20 (FEI, USA)), scanning electron microscope (SEM, Hitachi-4800 (Japan)). The composition of the obtained NPs is directly analyzed by high-angle annular dark field scanning transmission electron microscopy (STEM) imaging.

Surface property. The zeta potentials of the as-prepared nanoparticles were evaluated by using dynamic light scattering (DLS) analyzer (Malvern Nano ZS90, UK), and the average value was tested with three times. X-ray photoelectron spectroscopy (VG, America) was performed to study the elemental composition, elemental state and structure of the as prepared metal-assisted core-shell plasma nanoparticle.

Supplementary results

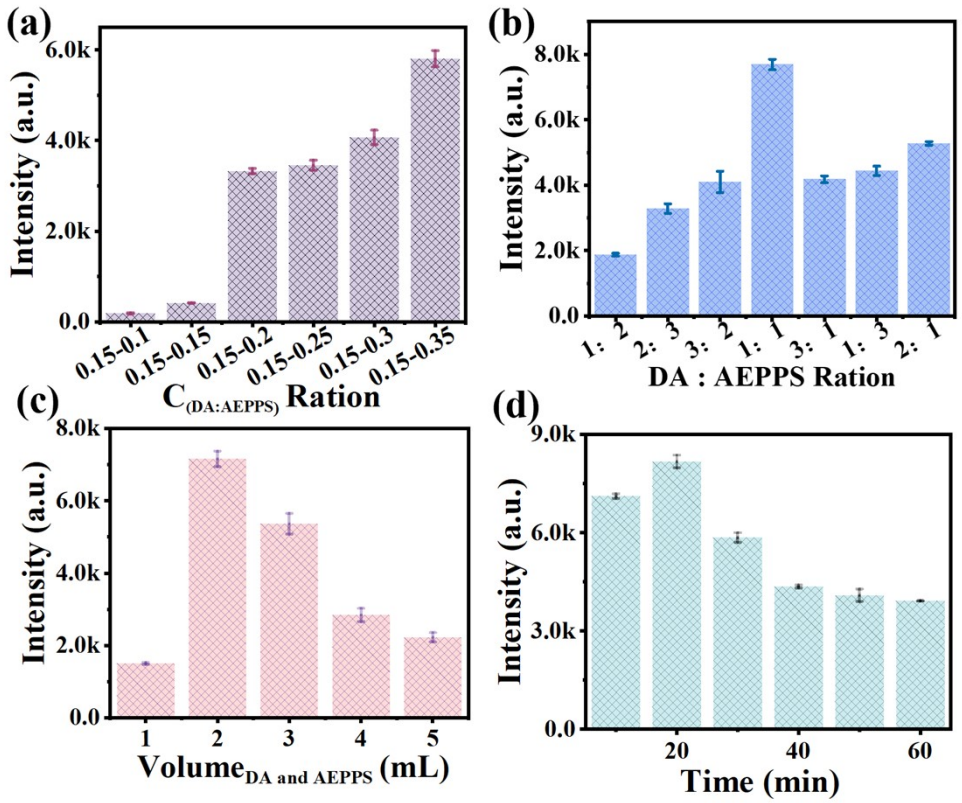

Figure S1. (a) DA and AEPPS reaction concentration ration(n=3) (b) DA and AEPPS reaction concentration volume ration(n=3) (c) DA and AEPPS volume(n=3) (d) DA and AEPPS reaction time effect on Raman spectral signal(n=3).

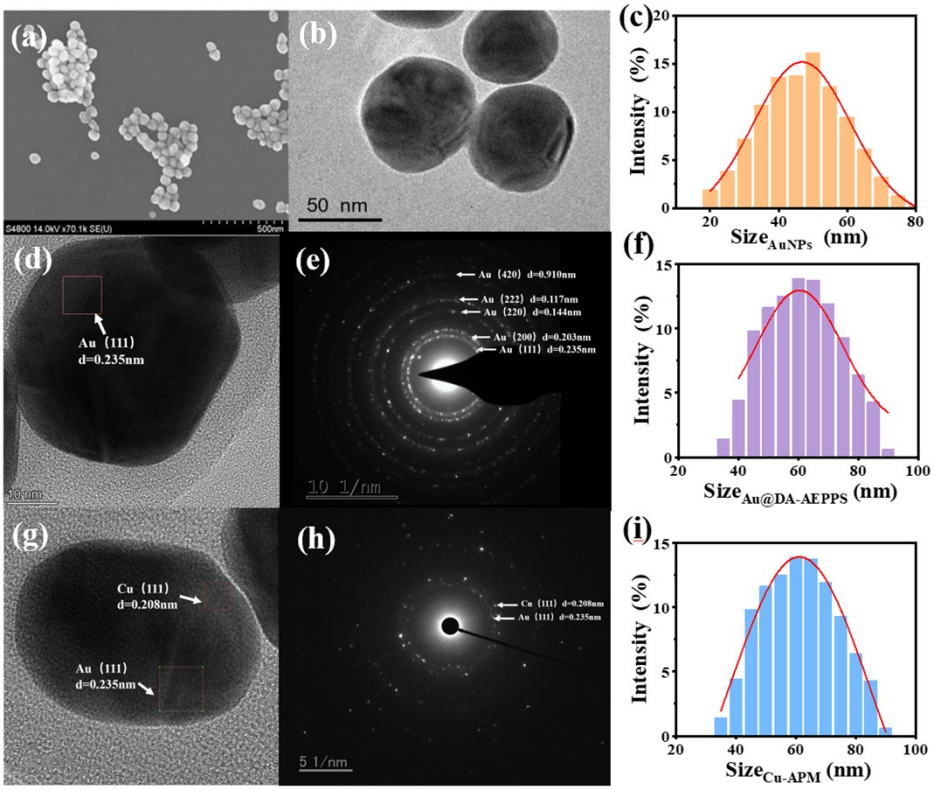

Figure S2. (a) SEM images of the Au NPs (b) TEM images of the Au NPs, (c) The size of Au NPs. (d)HRTEM images of the Au@DA-AEPPS NPs. (e) The SAED of Au@DA-AEPPS NPs. (f) The size of Au@DA-AEPPS NPs by the DLS studies. (g) HRTEM images of the Cu-APM. (h) The SAED of Cu-APM. (f) The size of Cu-APM by the DLS studies.

Table S1. The elements analyzed by XPS and EDS.

Element Amount	Cu	Au	C	N	O
XPS	6.28%	9.17%	50.29%	13.92%	20.34%
EDS	6.13%	8.34%	49.56%	15.78%	20.19%

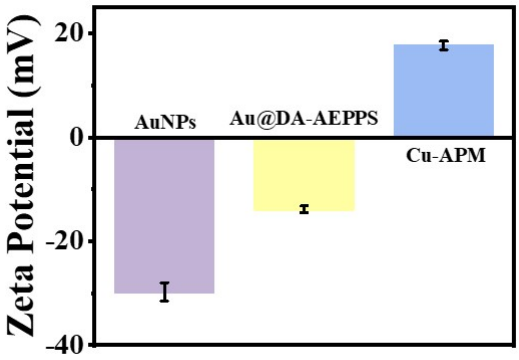

Figure S3. Zeta potentials of Au NPs, Au@DA-AEPPS NPs, Cu-APM(n=3).

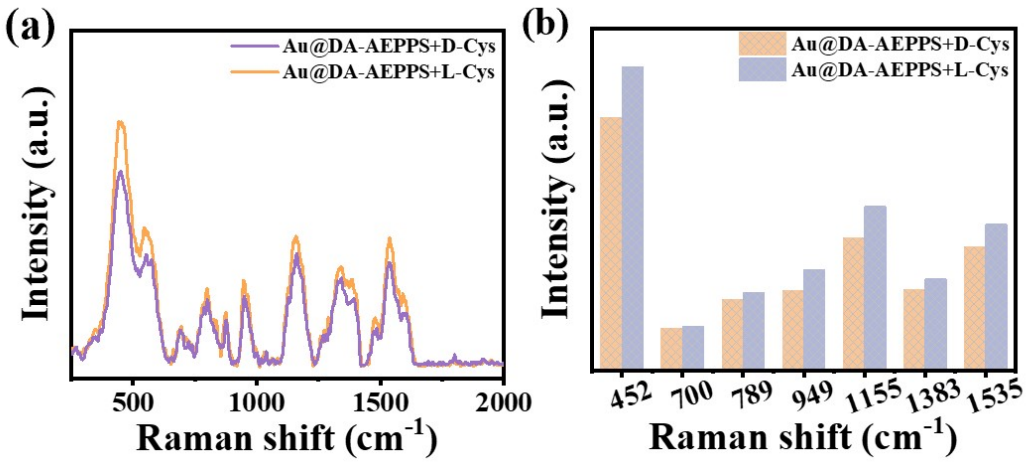

Figure S4. (a) Raman spectral behaviors of the L/D-Cys with Au@DA-AEPPS NPs. (b) Comparison of Raman intensity of L/D-Cys with Au@DA-AEPPS NPs.

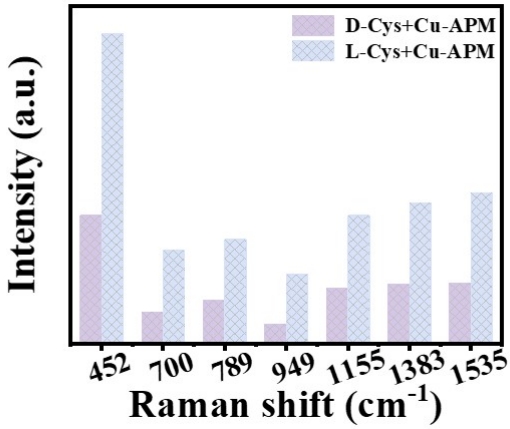

Figure S5. Comparison of Raman intensity of L/D-Cys with Cu-APM.

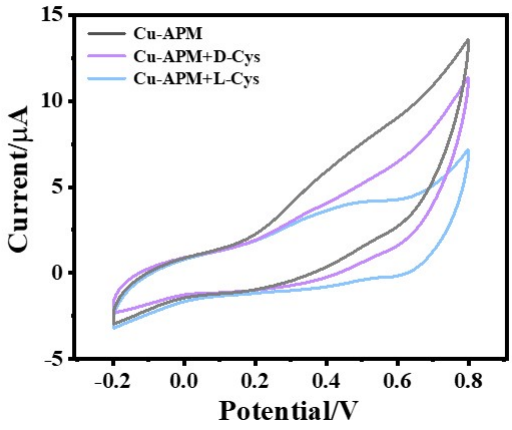

Figure S6. The CV responses of bare Cu-APM, Cu-APM+D-Cys, Cu-APM+D-Cys in electrolyte.

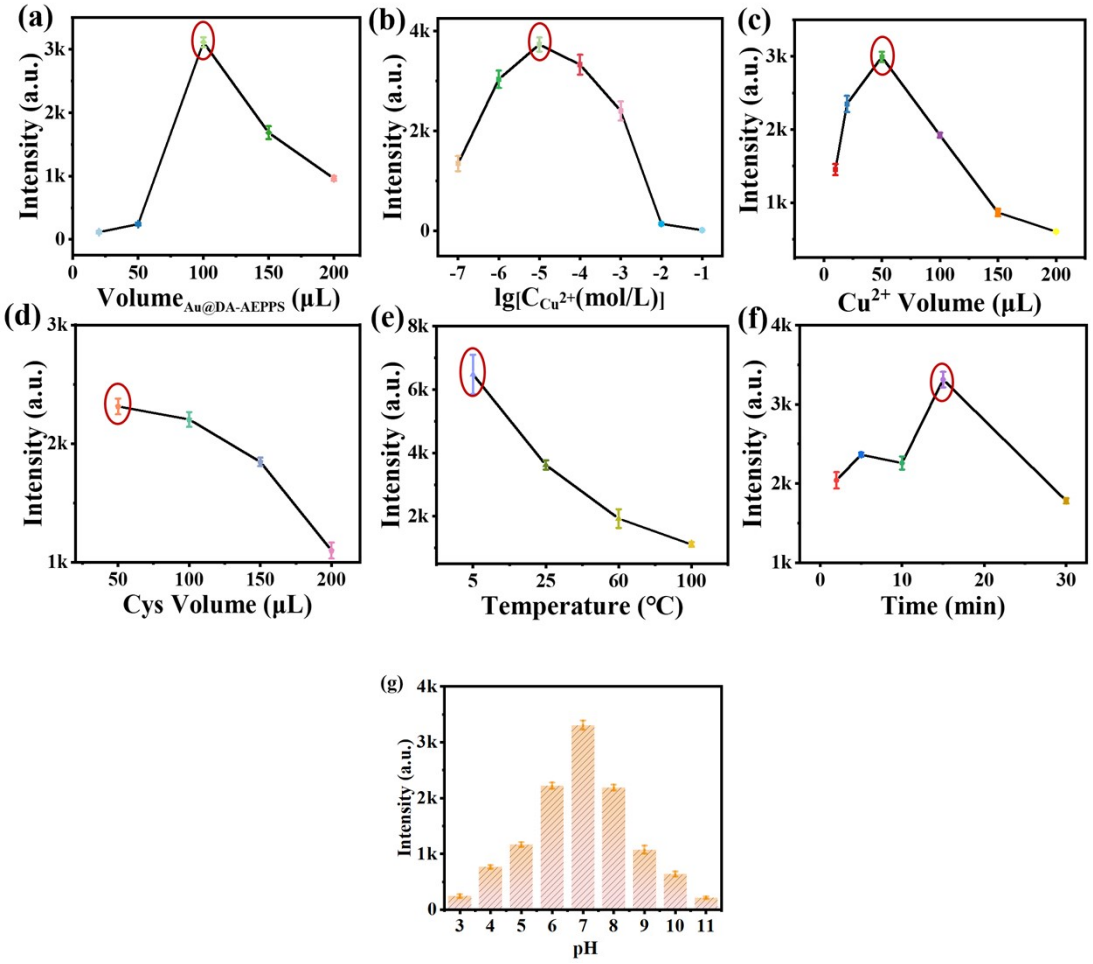

Figure S7. (a) Au@DA-AEPPS volume(n=3) (b) Cu^{2+} concentration(n=3) (c) Cu^{2+} volume (d) Cys volume(n=3) (e) reaction temperature(n=3) (f) reaction time, (g) pH, effect on Raman spectral signal(n=3).

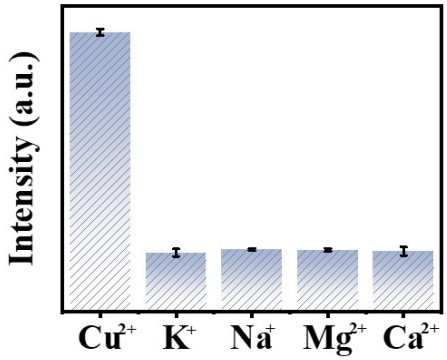

Figure S8. The SERS response of 479^{-1}cm to 10 μM of $Cu^{2+}$and 1 mM others (n=3).

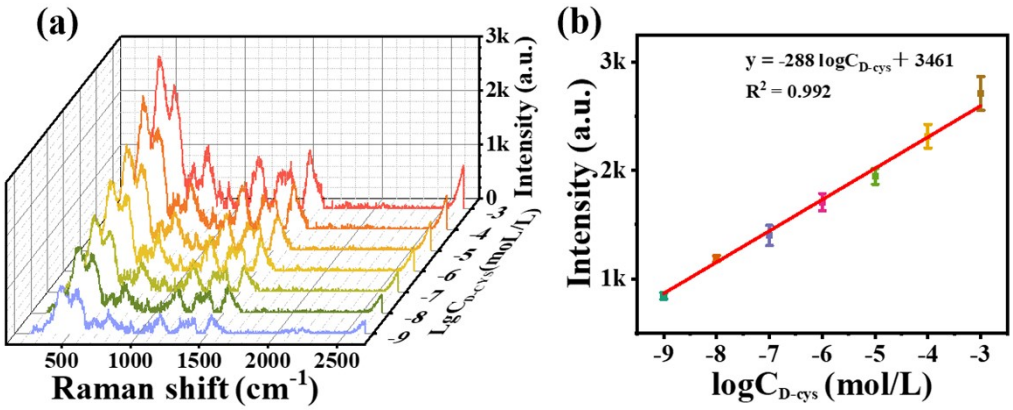

Figure S9. (a) SERS spectra of the system at different concentrations of D-Cys (10^{-3}-10^{-9} M). (b) Calibration plots based on the Raman intensity of 479 cm^{-1} with $C_{D\text{-}Cys}$(n=3).

Table S2. The performance of cysteine chiral enantiomers detected by biosensors with or without Cu^{2+} was compared.

Materials	Line Range (L-Cys/D-Cys)	LOD (L-Cys/D-Cys)
Au@DA-AEPPS	10^{-1}-10^{-7}M/-	78.4 nM/-
Cu-APM	10^{-3}-10^{-9} M 10^{-3}-10^{-9} M	0.77 pM/0.82 pM

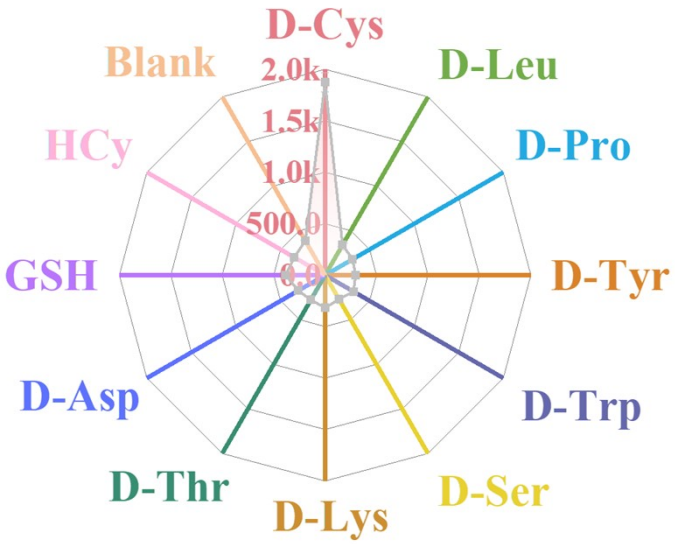

Figure S10. The SERS response of 479cm^{-1} to 10 μM of D-Cys and 1 mM others(n=3).

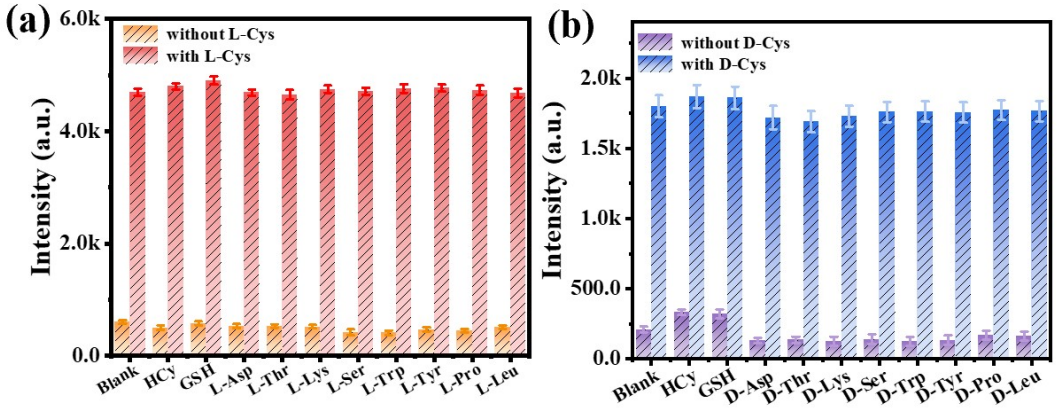

Figure S11. The SERS response of 479cm−1 to 10 μM of D-Cys and 1 mM others(n=3).

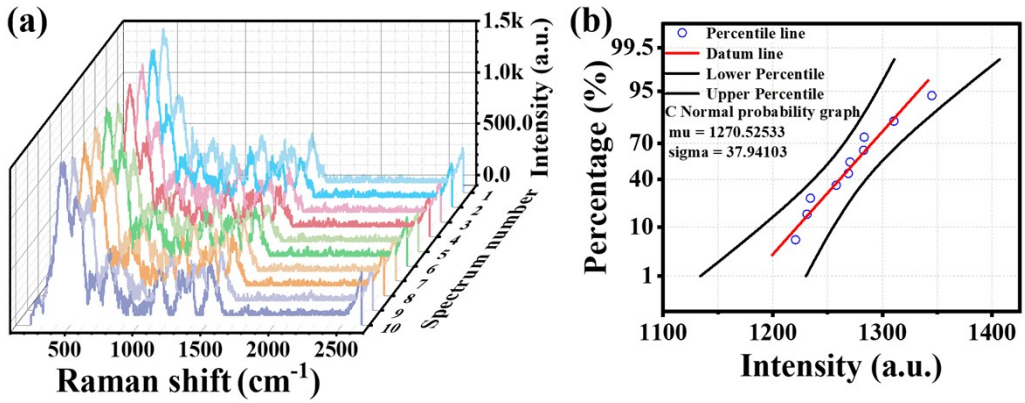

Figure S12. (a) SERS response of 479 cm^{-1} to 1mM of D-Cys with ten times. (b) C-normal probability plot for 10 different D-Cys.

Table S3. The performance of the Cu-APM biosensor for cysteine chiral enantiomer detection was compared with other detection methods.

Materials	Method	Line Range (L-Cys/D-Cys)	LOD (L-Cys/D-Cys)	Reference
Asn-CDs+Co^{2+}	Fluorescent	1.82-625 μM /—	0.61 μM/—	1
GSH-AuNCs	Fluorescent	0.50-100 mM 0.50-100 μM	0.36 μM/0.36 μM	2
Ag@mSiO_2	CD	20.0-100 μM 20.0-100 μM	12.5 μM /12.5 μM	3
Fe_3O_4@PDA/Cu_xO	ECL	0.01-5.00 μM 0.01-500 μM	83 pM/—	4
Ag-Au-ME	ECL	0.01-1.8μM/—	8.7 nM/—	5
RH/LH-S3/Ag	SERS	10 nM-100 μM 10 nM-100 μM	—	6
Cu-APM	SERS	1 nM-1 mM 1 nM-1 mM	0.77 pM/0.82 pM	This Work

Table S4. Determination results of D-Cys in food samples (n = 3).

Sample	Added (μM)	Proposed Method			HPLC Method			P*
		Detected (μM)	Recovery (%)	RSD (%)	Detected (μM)	Recovery (%)	RSD (%)	
Black garlic	0	1.87±0.22	—	—	1.76±0.15	—	—	0.93
	5.00	6.72±0.42	97	6.3	6.94±0.23	103.6	3.3	
	10.00	11.55±0.13	96.8	1.1	11.32±0.16	95.6	1.4	
Vinegar	0	1.74±0.25	—	—	1.66±0.19	—	—	
	5.00	6.81±0.41	101.4	6.0	6.23±0.27	91.4	4.3	
	10.00	12.38±0.33	106.4	2.7	11.87±0.22	102.1	1.9	
Beer	0	1.64±0.27	—	—	1.75±0.21	—	—	
	5.00	6.78±0.14	102.8	2.1	6.43±0.18	93.6	2.8	
	10.00	11.39±0.63	97.5	5.5	11.28±0.14	95.3	1.2	
Chess	0	1.21±0.16	—	—	1.15±0.26	—	—	
	5.00	6.05±0.23	96.8	3.8	6.31±0.13	103.2	2.1	
	10.00	11.38±0.27	101.7	2.4	10.88±0.17	97.3	1.6	

*The figured means of a t-test statistical analysis between two methods P>0.05, indicate no significant difference.

References

1. A. Chen, Y. Zhong, X. Yin, R. Li, Q. Deng, R. Yang, *Sens. Actuators, B.,* 2023, **393**, 134262.
2. S. Ruan, Y. Zhou, M. Zhang, H. Zhang, Y. Wang, P. Hu, *Anal. Sci.,* 2022, **38**, 541-551.
3. J. Wang, S.S. Zhang, X. Xu, K.X. Fei, Y.X. Peng, *Nanomaterials-basel.,* 2018, **8**, 1027.
4. H.F. Zhou, G.X. Ran, J.F. Masson, C. Wang, Y. Zhao, Q.J. Song, Rational design of magnetic micronanoelectrodes for recognition and ultrasensitive quantification of cysteine enantiomers, *Anal. Chem.,* 2018, **90**, 3374-3381.
5. H.F. Zhou, R.P. Yu, G.X. Ran, S. Moussa, Q.J. Song, J. Mauzeroll, J.F. Masson, *Sens. Actuators, B.,* 2020, **319**, 128315.
6. O. Guselnikova, R. Elashnikov, V. Svorcik, M. Kartau, C. Gilroy, N. Gadegaard, M. Kadodwala, A.S. Karimullah, O. Lyutakov, *Nanoscale Horiz.,* 2023, 8, 499-508.